Biomaterials 232 (2020) 119719

Contents lists available at ScienceDirect

Biomaterials

journal homepage: www.elsevier.com/locate/biomaterials

Magnesium oxide-crosslinked low-swelling citrate-based mussel-inspired tissue adhesives

Xili Lu[a,b,1], Sanjun Shi[c,1], Hanmei Li[d], Ethan Gerhard[b], Zhihui Lu[e,f], Xinyu Tan[f], Wenliang Li[g], Kevin M. Rahn[b], Denghui Xie[f], Guodong Xu[a], Fang Zou[a], Xiaochun Bai[f,h], Jinshan Guo[b,e,f,**], Jian Yang[b,*]

[a] Institute of Materials Processing and Intelligent Manufacturing, College of Materials Science and Chemical Engineering, Harbin Engineering University, Harbin, 150001, China
[b] Department of Biomedical Engineering, Materials Research Institute, The Huck Institutes of the Life Sciences, The Pennsylvania State University, University Park, PA, 16802, USA
[c] Center of Nanomedicine and Department of Department of Anesthesiology, Brigham and Women's Hospital and Harvard Medical School, Boston, MA, 02115, USA
[d] Key Laboratory of Coarse Cereal Processing (Ministry of Agriculture and Rural Affairs), College of Pharmacy and Biological Engineering, Chengdu University, Chengdu, 610106, China
[e] Department of Histology and Embryology, School of Basic Medical Sciences, Southern Medical University, Guangzhou, 510515, China
[f] Academy of Orthopedics, Provincial Key Laboratory of Bone and Joint Degenerative Diseases, The Third Affiliated Hospital of Southern Medical University, Guangzhou, Guangdong Province, 510280, China
[g] Center for Nanomaterials, School of Pharmacy, Jilin Medical University, Jilin, Jilin, 132013, China
[h] Department of Cell Biology, Key Laboratory of Mental Health of the Ministry of Education, School of Basic Medical Sciences, Southern Medical University, Guangzhou, 510515, China

ARTICLE INFO

Keywords:
Magnesium oxide (MgO)
Mussel-inspired adhesion
Citrate
Tissue adhesives
Wound closure

ABSTRACT

Tissue adhesives are commonly used in surgeries and regenerative engineering for the repair and regeneration of topical and internal wounds on tissues and organs such as skin, heart, blood vessels, and bone. However, achieving rapid crosslinking, strong wet adhesion and cohesion strengths, and minimal cytotoxicity remains a critical roadblock for clinical translation. Herein, in contrast to harsh and cytotoxic oxidants, magnesium oxide (MgO) particles were found to facilitate rapid crosslinking for injectable citrate-based mussel-inspired tissue bioadhesives synthesized by reacting citric acid, PEG-PPG-PEG diol and dopamine (iC-EPE). Our results confirmed the role of MgO particles as both crosslinkers and composite fillers to concurrently enhance bioadhesive cohesion and adhesion. iC-EPE crosslinked by MgO with/without sodium periodate (PI) exhibit enhanced mechanical strengths (1.0 Mpa $<$ tensile strength $\leq$ 4.5 MPa) compared to that of iC-EPE crosslinked only by PI (~0.75 MPa), high adhesion strength (up to 125 kPa, 8 fold that of fibrin glue (~15 kPa)), tunable degradability (full degradation from $<$ 1 week to $>$ 1 month), excellent *in vitro* and *in vivo* biocompatibility, encouraging anti-bacterial performance, and favorable wound closure efficacy. Thus, MgO crosslinked bioadhesives possess great potential for a wide range of applications in surgery and regenerative engineering.

1. Introduction

Tissue (bio)adhesives have attracted increased attention in recent years due to their wide applicability in the biomedical field, including wound closure, hemostat, tissue sealing, implant fixation, and drug delivery [1–6]. Commercially available biologically-derived fibrin glue (*Tisseel*), which is mainly composed of concentrated fibrinogen, thrombin, and calcium chloride thus duplicating the last stage of biological coagulation cascade, is the most widely used tissue adhesive due to its fast curing and biodegradability and often considered as the gold standard of tissue adhesives. However, there are also limitations such as poor wet tissue adhesion, thus reducing its efficacy for applications where strong tissue adhesion is required [3,6,7]. Cyanoacrylate adhesives offer advantages such as ease of use, strong adhesion to tissue

* Corresponding author.
** Corresponding author. Department of Biomedical Engineering, Materials Research Institute, The Huck Institutes of the Life Sciences, The Pennsylvania State University, University Park, PA, 16802, USA.
E-mail addresses: jsguo4127@smu.edu.cn (J. Guo), jxy30@psu.edu (J. Yang).
[1] These authors contributed equally to this work.

https://doi.org/10.1016/j.biomaterials.2019.119719
Received 8 September 2019; Received in revised form 26 November 2019; Accepted 20 December 2019
Available online 23 December 2019
0142-9612/

[3,6,8]. However, the applications of cyanoacrylates have been mainly limited to topical uses due to the concerns such as slow degradation, exothermic polymerization, and toxicity of degradation products. Albumin-glutaraldehyde bioadhesive (*BioGlue*) is clinically used in cardiac and vascular repair and pulmonary repair, but it also brings a concern on its toxicity due to the use of a toxic crosslinking component [9,10]. Urethane-based (*TissuGlu*) tissue adhesives may offer strong tissue adhesion and fast curing, but they may suffer from vigorous exothermic chemical reactions and slow degradation [8,11]. Poly (ethylene glycol) (PEG)-based bioadhesives, such as *CoSeal* and *DuraSeal*, have been successfully used as tissue sealants for some applications, but concerns on their large swelling ratios and rapid degradation were believed to possibly trigger significant post-surgical complications such as rapid leakage, compression on the nearby nerve ends, and the formation of hematoma [12,13].

In order to address these limitations, intensive efforts have been expended in the development of new bioadhesives with superior biocompatibility and strong wet tissue adhesion strength. Inspired by the strong adhesion of marine mussels to multiple heterogeneous surfaces under water, mussel-inspired bioadhesives have been developed by incorporating L-DOPA (L-3,4-dihydroxyphenylalanine) or dopamine into polymers to achieve enhanced wet tissue adhesion and biocompatibility [2,14–20]. In our lab, a family of biodegradable, injectable, citrate-based mussel-inspired bioadhesives (iCMBAs, or iCs) has been developed via a facile one-step polycondensation of citric acid (CA), PEG, dopamine, and other functional moieties [2,15–17], benefiting from versatile citrate chemistry [21–23]. Tested iCMBA formulae demonstrated strong tissue adhesion strengths in the range of 30–215 kPa (lap shear strength), 2.5–13.0 times stronger than that of the gold standard fibrin glue (~15 kPa). However, harsh oxidants, such as sodium periodate (PI), silver nitrate (SN), and iron (III) chloride ($FeCl_3$) used to crosslink these materials generated significant toxicity concerns. Additionally, constituted with hydrophilic PEG, crosslinked iCMBAs possess high swelling ratios (up to > 1000 wt%) [15–17].

Herein, to reduce the swelling ratio, a more hydrophobic iCMBA prepolymer (iC-EPE) was synthesized by a facile one-pot polycondensation reaction of CA, poly(ethylene glycol)-block-poly(propylene glycol)-block-poly(ethylene glycol) (PEG-PPG-PEG) diol and dopamine (DP). iC-EPE is soluble in a mixed ethanol/water solvent system (Scheme 1A). Although water-based materials are typically preferred *in vivo*, incorporation of ethanol in iC-EPE formulation was considered beneficial due to ethanol's previous use as a topical antimicrobial agent as well as the most effective treatment of venous malformation [24]. Ethanol was also used in combination with a recently approved polyurethane-based tissue bioadhesive, *TissuGlu*, for abdominoplasty to prevent postoperative seroma formation by promoting scab formation between two tissue layers [25,26].

Unexpectedly, MgO particles were also found to crosslink iC-EPE or other iCMBAs through simple mixing. Mg is a biocompatible trace metal ion ubiquitous throughout the human body, and is one of the main components of the inorganic ceramic of bone. It has been reported that Mg ions play an important role in mediating the functions of all cells in the body and promoting cell attachment, proliferation and migration [27]. Additionally, Mg ions can also mediate cell-extracellular matrix interactions and regulate bone apatite structure and density [27]. Furthermore, MgO is known to exhibit antibacterial properties [28,29]. Thus, MgO particles can act as both crosslinking initiators (biocompatible oxidant) and composite fillers in the first instance, to simultaneously enhance the cohesion and adhesion strengths of these bioadhesives, and as a bioactive component promoting antibacterial and regulating cellular activities over the lifetime of the composite. These features support the potentials of iC-EPE-MgO to be used in many surgical circumstances such as topical skin closure and healing or internal wound closure and healing, and injectable bone fillers. Critically, using MgO as a crosslinking initiator eliminates the use of toxic oxidants such as PI and SN. A systemic investigation was conducted and possible crosslinking mechanisms were proposed. The effects of MgO incorporation in iC-EPE adhesives on the curing time, mechanical properties, degradation profile, *in vitro* and *in vivo* biocompatibility, anti-bacterial activity, as well as *in vivo* wound closure and regeneration efficacy of the composite bioadhesives were also evaluated.

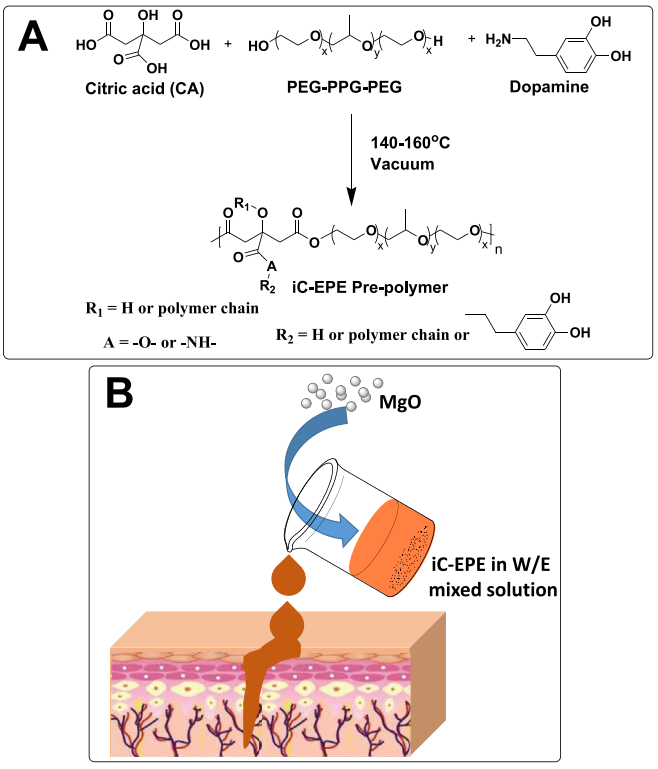

Scheme 1. (**A**) Synthesis of iC-EPE (injectable citrate-based mussel-inspired bioadhesives (iCMBAs, iC) made with PEG-PPG-PEG (EPE) diol) prepolymers; (**B**) Magnesium oxide (MgO) serves both as a crosslinker and a composite filler to enable a wide tunability on the crosslinking time and the adhesion strengths of the resultant iC-EPE/MgO hydrogels that hold great potential for a myriad of surgical applications such as wound closure and healing.

2. Experimental section

2.1. Materials

All reagents and solvents, including magnesium oxide (MgO, Lot # MKBS7178V, ~325 mesh), poly(ethylene glycol)-block-poly(propylene glycol)-block-poly(ethylene glycol) (PEG-PPG-PEG, Pluronic® L-31, with an average molecular weight of 1100 Da), and dopamine, were purchased from Sigma-Aldrich and used without further purification unless otherwise specified.

2.2. Synthesis and characterization of iC-EPE prepolymers

The iC-EPE prepolymer was synthesized by the polycondensation of citric acid (CA), PEG-PPG-PEG and dopamine (DP) as reported previously (Scheme 1A). Briefly, CA, PEG-PPG-PEG and DP (molar ratio = 1.2: 1.0: 0.3) were placed in a one-necked round-bottom flask equipped with a vacuum stopper, and the mixture was heated to 160 °C under stirring until complete melting was observed. Then, the temperature was reduced to 140 °C and the reaction was continued under vacuum until the stir bar stopped turning at 60 rpm. The reaction mixture was dissolved in ethanol and precipitated in extensive deionized (DI) water and then was lyophilized to obtain the purified iC-EPE prepolymer.

Fourier transform infrared (FTIR) spectra of iC-EPE and normal iC-P_{400} (iCMBA-$P_{400}D_{0.3}$, synthesized according our previous work [15,17]), were obtained with a Nicolet 6700 FTIR spectrometer to characterize the functional groups of the prepolymers. Prepolymer solutions in acetone were cast onto KBr plates and the solvent was evaporated, with blank KBr used as background. ^{1}H NMR spectra of prepolymers in DMSO-d_6 were recorded on a 300 MHz Bruker DPX-300 FT-NMR spectrometer. The dopamine content of prepolymer was determined by UV–vis spectra using a Shimadzu UV-2450 spectrophotometer with a minimum wavelength resolution of 0.2 nm.

2.3. Preparation of iC-EPE/MgO composite hydrogels and gel time test

The iC-EPE prepolymer was dissolved in mixed solution (ethanol: DI water = 80:20, w/w) to form a 40 wt% polymer solution, and then 5, 10, 15, or 20 wt% (weight percent to dry polymer) of MgO powder was dispersed in DI water, ethanol or sodium periodate (PI) solution (dissolved in DI water) and used as crosslink initiator. iC-EPE/MgO composite hydrogels were fabricated by mixing polymer solution and MgO dispersion with a volume ratio of 2: 1. Unless specified otherwise, all hydrogels were allowed to cure for 24 h and then freeze-dried for at least 2 days for further characterization. The gel times of different samples were measured via tilting test. For each sample, testing was conducted three times to obtain the average values.

The sample names of iC-EPE prepolymer crosslinked by different amounts of MgO, different solvent/solution used to disperse MgO, and with/without PI, are shown in Table 1.

2.4. Rheological testing of iC-EPE/MgO composite hydrogels

Rheological tests were carried out using a Discovery Series Hybrid Rheometer (DHR-1, TA Instruments, USA) in a parallel plate configuration, employing sandblasted stainless steel 40 mm diameter plates throughout and a Peltier plate for temperature control. 2 mL iC-EPE prepolymer solution (40 wt%) and 1 mL crosslink initiator dispersion (10 wt% MgO dispersed in DI water, ethanol or 8 wt% PI solution) was mixed, and the mixture was immediately deposited on the lower plate of the rheometer. The upper plate was immediately brought down to a gap distance of 40 μm and both storage (G′) and loss (G″) modulus values as a function of time were recorded at a frequency of 1 Hz and a strain of 1%. Each measurement was performed three times. The gel time was approximated by the G′/G'' crossover time.

2.5. Characterization of physical properties of iC-EPE/MgO composite hydrogels

Mechanical properties of dried iC-EPE composite hydrogel films were measured on an Instron 5966 machine with a 1 kN (for dried films) or 10 N (for swollen films) load cell (Instron, Norwood, MA) according to ASTM D412A. Dumbbell-shape samples (25 mm × 6 mm × 1.5 mm, length × width × thickness) were pulled to failure under a stain rate of 500 mm/min. Elastic modulus, tensile stress and elongation at break were recorded for various films as the average of eight repeats. In order to evaluate the effect of hydration on the mechanical properties of iC-EPE composite hydrogels, the mechanical tests were also conducted on samples after being hydrated in wet conditions for 48 h.

The sol content and swelling ratio of crosslinked iC-EPE/MgO composite hydrogels were measured as described previously [15–17] and then calculated using equations (1) and (2), respectively.

$$Sol\ content\,(\%) = \frac{W_i - W_d}{W_i} \times 100 \tag{1}$$

$$Swelling\ ratio\,(\%) = \frac{W_s - W_d}{W_d} \times 100 \tag{2}$$

where W_i denotes the initial mass of dry iC-EPE hydrogel sample, W_d represents the mass of freeze-dried sample after leaching the uncrosslinked part with 1, 4-dioxane for 48 h, and W_s represents the mass of network sample blotted dry with filter paper after suspending in water for 24 h.

Degradation profiles were evaluated by *in vitro* degradation in phosphate buffered saline (PBS, pH 7.4, 01 M) at 37 °C. Disc specimens (7 mm in diameter, 1 mm thick) were accurately weighed (W_o) and then were immersed in 10 mL of PBS and incubated at 37 °C. The PBS solution was changed every other day. At a pre-determined time point, samples were thoroughly washed with DI water and freeze-dried to determine the residual mass (W_t). Mass loss was calculated using equation (3):

$$Mass\ loss\,(\%) = \frac{W_0 - W_t}{W_0} \times 100 \tag{3}$$

2.6. Adhesion strength of iC-EPE/MgO composite hydrogels

The adhesion strength of iC-EPE composite hydrogels was determined by the lap shear strength test according to the modified ASTM D1002-05 method. Porcine-derived, acellular small intestine submucosa (SIS) material (OASIS®, HealthPoint Ltd. Fort Worth, TX) was cut into 40 mm × 4 mm strips and hydrated in PBS for at least 1 h before testing. After mixing the iC-EPE prepolymer solution with predetermined amounts of crosslink initiator, 10 μL of the mixture was added and spread over one end of a strip. A second wet strip was subsequently placed in contact with the first one to form an overlapping area of 6 mm × 4 mm. The adhered strips were compressed with a 100g weight for 20 min and then were placed in a highly humid chamber for 2 h prior to testing. The lap shear strength of bonded strips was subsequently measured using Instron 5966 fitted with a 10 N load cell at a rate of 1.3 mm/min. The lap shear strength of fibrin glue (*Tisseel*, Baxter healthcare Corp.) was used for comparison.

2.7. In vitro biocompatibility tests

The *in vitro* biocompatibility of the cross-linked iC-EPE/MgO composite hydrogels was assessed by testing cell cytotoxicity of the sol contents (or leachable fractions) and degradation products, following

Table 1
Nomenclature of different iC-EPE composite hydrogels crosslinked by different MgO contents, different MgO dispersing solvent/solution, and with/without sodium (meta) periodate (PI). These composite hydrogels were all crosslinked at room temperature.

Sample[a]	W5/10/15/20	E5/10/15/20	8PI	W5/10/15 + 2/4/8PI
MgO (wt%)[b]	5/10/15/20	5/10/15/20	0	5/10/15
Solvent/Solution[c]	DI water	Ethanol	8 wt% PI	2/4/8 wt% PI

[a] To crosslink iC-EPE prepolymer, the iC-EPE prepolymer was dissolved in ethanol/water (80/20, w/w) into a 40 wt% solution, and MgO was dispersed in the solvent/solution as shown in the table. The volume ratios between polymer solution and MgO dispersion were all 2/1 (v/v)

[b] MgO to composite ratio, MgO was dispersed in water (W), ethanol (E), PI solution, or the combination of MgO and PI in water. W5/10/15/20 are a series of hydrogels of W5, W10, W15, and W20, similar for the others.

[c] Solvent/solution that MgO was dispersed in.

the same process as described in our previous work [1–3]. Human-derived mesenchymal stem cells (hMSC, ATCC® PCS-500-012TM, from ATCC, passage 5–10) were used.

The cytotoxicity of the sol contents of crosslinked iC-EPE/MgO composite hydrogels was studied using MTT (methylthiazolyl-diphenyl-tetrazolium bromide) assay against hMSCs. The leachant (sol content) solution of the hydrogel was obtained by incubating 0.5 g dried hydrogel specimens in 5 mL of PBS (pH 7.4) at 37 °C for 24 h. Next, three different dilutions were prepared: 1 × , 10 × and 100 × (1 × was the solution of leached products without dilution; 10 × and 100 × were 10 times and 100 times diluted from 1 × solution with PBS, respectively). To each well of a 96-well cell culture plate, 200 μL of hMSC solution in growth medium (composed of Dulbecco's modified eagle's medium (DMEM), 10% (v/v) fetal bovine serum (FBS) and 1% (v/v) antibiotic antimycotic solution (100×)) with a density of 5 × 10^4 cells/mL was added and incubated for 24 h. Then, 20 μL of sol content solution with various concentrations were added and the cells were incubated for another 24 h followed by MTT assay.

The cytotoxicity of degradation products of hydrogels was also evaluated. Equal weight (1 g) of dried iC-EPE/MgO hydrogel samples as well as FDA (Food and Drug Administration)-approved poly (lactic-co-glycolic acid) (PLGA, used as control, LA/GA = 50/50, Mw~60 KDa, purchased from Polyscitech) were fully degraded in 10 mL of 0.2 M NaOH solution. After adjusting pH to 7.4, the resultant solutions were diluted to three concentrations (1 × , 10 × and 100 ×) using PBS (pH 7.4), and used for cell culture (the process was the same as used in the sol content cell cytotoxicity study described above) and subsequent MTT analysis.

Cell adhesion and proliferation on iC-EPE composite hydrogels films was also studied against hMSC cells and the cell morphology was observed by Live/Dead staining assay, using W10 as an example. Briefly, 20 μL of iC-EPE prepolymer solution was mixed with 10 μL of MgO DI water solution (0.088 g/mL), and the mixture was uniformly spread on the surface of a glass slide to form a thin film of W10 with a diameter of 15 mm prior to completion of cross-linking. Then the samples were sterilized by incubation in 70% ethanol for 24 h followed by exposure to UV light for 3 h. After that, the samples were placed in 24-well plates and seeded with 500 μL hMSC solution with a density of 5000 cells/cm^2 followed by growth medium replacement the next day. At pre-determined time points (cells were incubated for 1, 3 and 7 days), the medium was removed from the well plate and the cells were washed with PBS then stained by Live/Dead Viability/Cytotoxicity Kit (Invitrogen, molecular probes, Eugene, OR) for the observation of cell morphology using an inverted light microscope (Nikon Eclipse Ti–U) equipped with a ANDOR DL-604M-#VP camera and Prior Lumen 200.

2.8. In vitro anti-bacterial properties of iC-EPE bioadhesives

The anti-bacterial properties of iC-EPE composite hydrogels were tested against *Staphylococcus aureus* (*S. aureus*) and *Escherichia coli* (*E. coli*) as positive and negative bacteria models respectively. *S. aureus* (ATCC® 6538TM) and *E. coli* (ATCC® 25922TM) were purchased from ATCC (American Type Culture Collection) and used according to established safety protocols. Tryptic soy broth (Cat. #: C7141) and tryptic soy agar (Cat. #: C7121) used for *S. aureus* culture were purchased from Criterion (via VWR). Luria broth base (LB broth, Cat. #: 12795–027) and select agar (Cat. #: 30391–023) used for *E. coli* culture were purchased from Invitrogen. *S. aureus* and *E. coli* mono-colonies were incubated in sterilized tryptic soy broth and LB broth, respectively, at 37 °C on an orbital shaker overnight and the obtained bacteria suspensions were diluted to desired concentrations prior to use.

W10, E10, W10 + 8PI and 8PI were selected as the representative experimental samples and PEGDA/HEMA (w/w = 1/1) was used as positive control. Firstly, bacteria suspension with an optical density (OD) of 0.07 at 600 nm was prepared. Then the bacteria suspension was diluted with broth medium 100 times to obtain the expected concentration. Colony counting was conducted to determine the bacteria concentration in CFUs (colony forming units) per milliliter. 0.2 g of freeze-dried samples (without removing leachable components) were immersed in 20 mL of the above bacteria suspension and incubated at 37 °C for 24 h on an orbital shaker. After that, the diluted medium was cast on an agar plate for colony counting. Bacteria growth broth was also tested and served as a negative control. The bacterial inhibition ratios of samples were calculated by equation (4):

$$\text{Inhibition ratio (\%)} = 100 - 100 \times \frac{N_t - N_0}{N_{con} - N_0} \quad (4)$$

where N_0 was the bacteria concentration in broth medium before incubation in the unit of CFUs/mL. N_t and N_{con} were the bacteria concentration of broth containing hydrogels and pure broth (control) after incubation for 24 h, respectively, also in the unit of CFUs/mL.

2.9. In vivo study

Skin incisions were made on Sprague-Dawley rats (female, 260 ± 50 g, n = 5) to evaluate the *in vivo* biocompatibility and wound healing performance of iC-EPE crosslinked by MgO (10 wt% in water, W10). All *in vivo* experiments were performed with the approval of the Third Military Medical University, China. Briefly, the rats were anaesthetized using 40 mg/kg of ketamine and the hair on the dorsal side was shaved. The skin surgical area on the dorsum was sterilized with 75% ethanol and then whole-layer surgical skin injuries were created (2 cm long × 0.5 cm deep). The sterilized iC-EPE was mixed with MgO (W10) and the adhesive was dropped into the wounds followed by finger-clamping for 5 min. In parallel, conventional sutures were used as positive control. On the 7th and 28th day post-administration, the treated skin wounds were harvested and fixed by 4% paraformaldehyde for histological study. Hematoxylin and eosin (H&E) staining and Masson trichrome staining were performed to assess the morphology and the collagen production, respectively. Immunohistochemistry for CD11b expression was also performed to evaluate inflammation. CD11b positive cells in the tissues were detected using rabbit anti-rat Integrin aM (H-61, Santa) and peroxidase-conjugated goat anti-rabbit secondary antibodies (Santa). The stained tissue sections were observed by light microscopy (Nikon, Tokyo, Japan). At different time points after treatment, the number of cells infiltrating into the incision area and the number of CD11b positive cells were calculated in random areas using Image J. Collagen density (%) was determined by calculating the ratio of blue-stained area to total area of Masson trichrome staining images using Image J. At least 5 random areas were selected and the results were averaged.

2.10. Statistical analysis

All data is presented as mean ± standard deviation, with tested sample number of at least 5. The significance of differences between results was evaluated by One-Way ANOVA test. A p value < 0.05 (*) was considered to be statistically significant.

3. Results and discussion

3.1. Synthesis and characterization of iC-EPE prepolymers

Original iCMBAs used hydrophilic PEG diols to confer water solubility. Thus, the crosslinked hydrogels possessed very high water swelling ratios, in extreme cases > 1000 wt% [15–17]. To reduce the swelling ratio, more hydrophobic PEG-PPG-PEG (EPE) was used to react with CA and dopamine via a convenient one-pot polycondensation to produce iC-EPE prepolymer (Scheme 1A). FTIR spectra of iC-EPE and iC-P_{400} (synthesized using PEG_{400}, for comparison) prepolymers are shown in Fig. 1A. The peak between 1700 and 1748 cm^{-1} was assigned to the carbonyl group (C═O) in the ester group. The peak at 1540 cm^{-1}

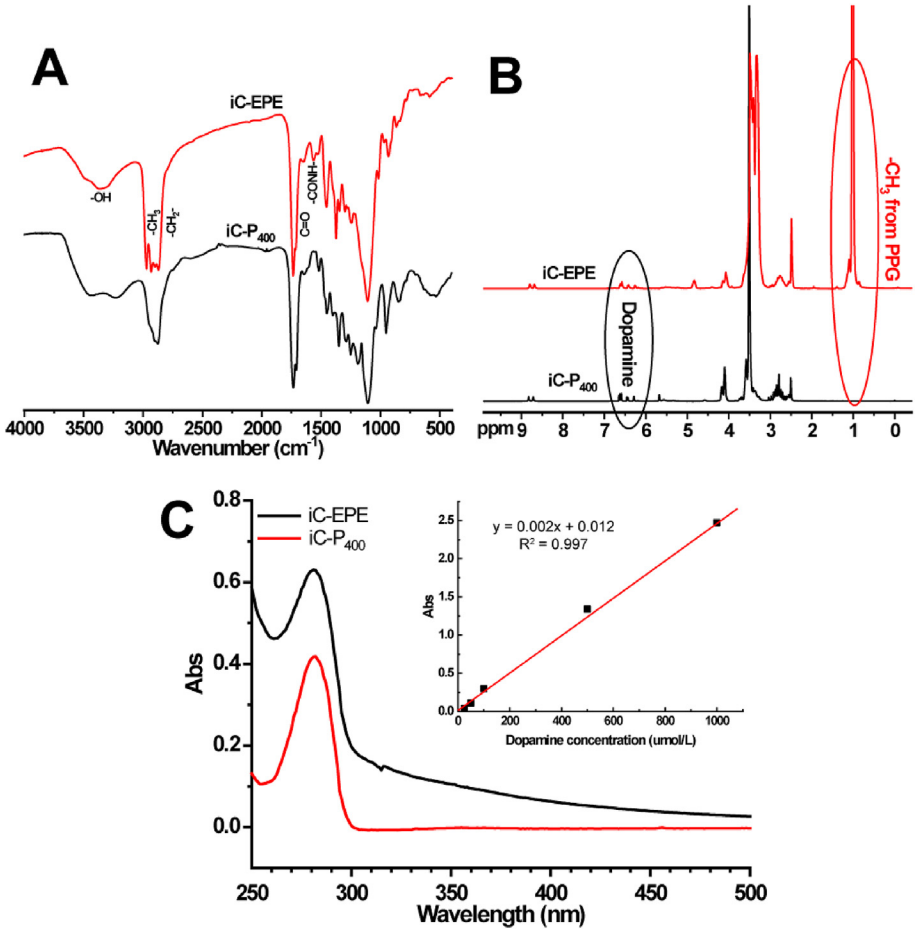

Fig. 1. Characterization of prepolymers: FTIR (**A**), ^{1}H NMR (**B**) and UV–vis absorption spectra (**C**) of 0.4 mg/mL of iC-EPE and iC-P_{400} (iCMBA composed of citric acid, poly(ethylene glycol) with a molecular weight of 400 Da (PEG_{400}), and dopamine) in ethanol/water mixed solvent (w/w = 40/60). The insert panel in **C** is the standard curve of dopamine in a mixed ethanol/water solvent (w/w = 40/60).

was assigned to the amide group (-C(=O)–NH-), which confirmed the formation of amide linkages between the –COOH groups of CA and $–NH_2$ groups of dopamine. The peaks around 2932 cm^{-1} and 2870 cm^{-1} were assigned to methyl ($-CH_3$) and methylene ($–CH_2–$) groups from PEG-PPG-PEG, respectively. The relatively broad peak at 3364 cm^{-1} was ascribed to the presence of hydroxyl groups. The ^{1}H NMR spectra of iC-EPE and iC-P_{400} are shown in Fig. 1B. The peak at 1.02 ppm in the iC-EPE spectrum not present in the ^{1}H NMR spectrum of iC-P_{400} was assigned to the protons of $–CH_3$ from EPE, the most characteristic peak of iC-EPE. The multiple peaks between 2.55 and 2.90 ppm were assigned to the protons in methylene groups from citric acid and dopamine. The chemical shifts at 6.40–6.70 ppm shown in the spectra of both iC-EPE and iC-P_{400} prepolymers were assigned to the protons of the phenyl group, characteristic of catechol group. The FTIR and ^{1}H NMR results further confirm the esterification reaction between CA and EPE, and the formation of amide linkages between the –COOH groups of CA and dopamine's $–NH_2$ group. The UV–vis spectrum further verifies the availability of catechol hydroxyl groups in the iC-EPE prepolymer via the UV absorption peak at 280 nm (Fig. 1C). Dopamine content in the iC-EPE prepolymer was determined to be 0.308 mmol/g according to the dopamine standard curve shown in the insert panel in Fig. 1C.

3.2. Preparation of iC-EPE/MgO composite hydrogels and gel time measurement

Catechol mediated crosslinking of polymers often utilize harsh and toxic water based oxidants, such as sodium (meta) periodate (PI), silver nitrate (SN), or $FeCl_3$. Alternatively, enzymes such as horseradish peroxidase (HRP) and mushroom tyrosinase (MT), while effective when used in the crosslinking of tyramine or tyrosine containing polymers [30], display long crosslinking times up to several hours, and often require large amounts of enzyme for crosslinking catechol group-containing polymers, thus reducing both practicality and cost effectiveness in such systems [31]. Currently, there are few reports for effective crosslinking of catechol group-containing polymers without the use of toxic oxidants.

For the first time, MgO particles were found to be capable of crosslinking iC-EPE or other iCMBAs by simply mixing them with MgO dispersions in water or ethanol (Scheme 1B). The effects of MgO content on the gel time of iC-EPE/MgO composite hydrogels are shown in Fig. 2A and Table S1. Gel time decreased with the increase of MgO content. Moreover, for the same MgO content, MgO dispersed in water crosslinked iC-EPE prepolymer faster than the equivalent amount of MgO dispersed in ethanol. The effects of temperature on gel time are shown in Fig. 2B. For equivalent MgO content, increased temperature resulted in an obvious decrease in gel time. For example, at 10 wt% MgO, the gel time decreased from 324 s at 25 °C (room temperature, RT) to 176 s at 37 °C (human body temperature). The gel times of MgO-induced iC-EPE crosslinking were in the range of 200–1300 s (Fig. 2A and B), with most gel times decreased compared to the gel time of iC-EPE crosslinked by pure 8 wt% PI (1568 ± 47s, Table S1), and comparable to the gel times of normal iCMBAs crosslinked by PI [15]. When mixing MgO and PI together in water, gel times significantly decreased to less than 60 s for all tested samples (Fig. 2C and Table S1). When the MgO content was kept the same, 2 wt% PI led to the fastest crosslinking, while further increasing PI concentration did not induce faster crosslinking. This may be caused by the mutual inhibition between MgO and PI. When the PI concentration was 2 wt%, it may have promoted the crosslinking of iC-EPE prepolymer by MgO, but when the PI

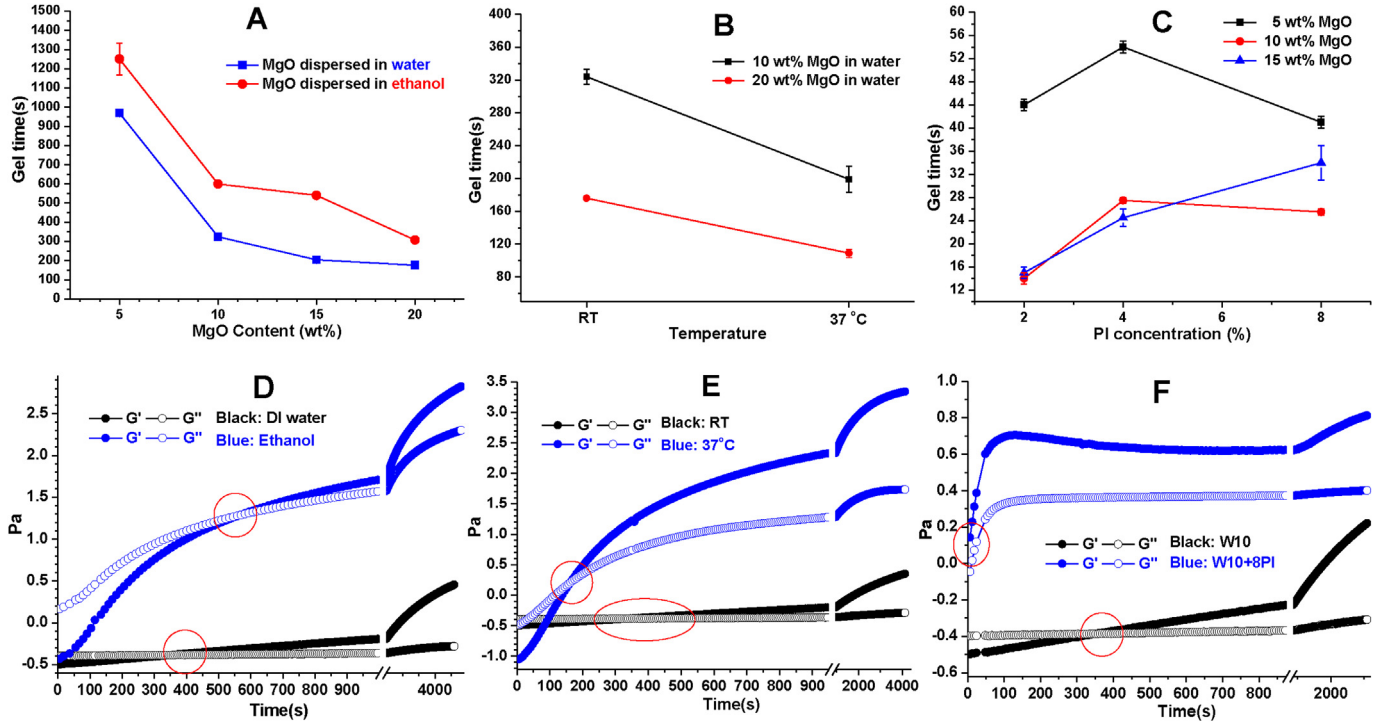

Fig. 2. Gelation (Gel) time determination: Gel times (obtained by tilting test) of iC-EPE crosslinked by MgO at different MgO concentrations (**A**), different temperatures (**B**), and different MgO/PI concentrations in water (**C**); Representative results of rheology tests for iC-EPE crosslinked by 10 wt% MgO dispersions in different solvents (ethanol or water, **D**), at different temperatures (MgO was dispersed in water, **E**), or crosslinked by mixed solutions of MgO and 8 wt% PI (**F**). The gel time was determined by the crossover point (red circle) of storage modulus (G′) and loss modulus (G″). (For interpretation of the references to colour in this figure legend, the reader is referred to the Web version of this article.)

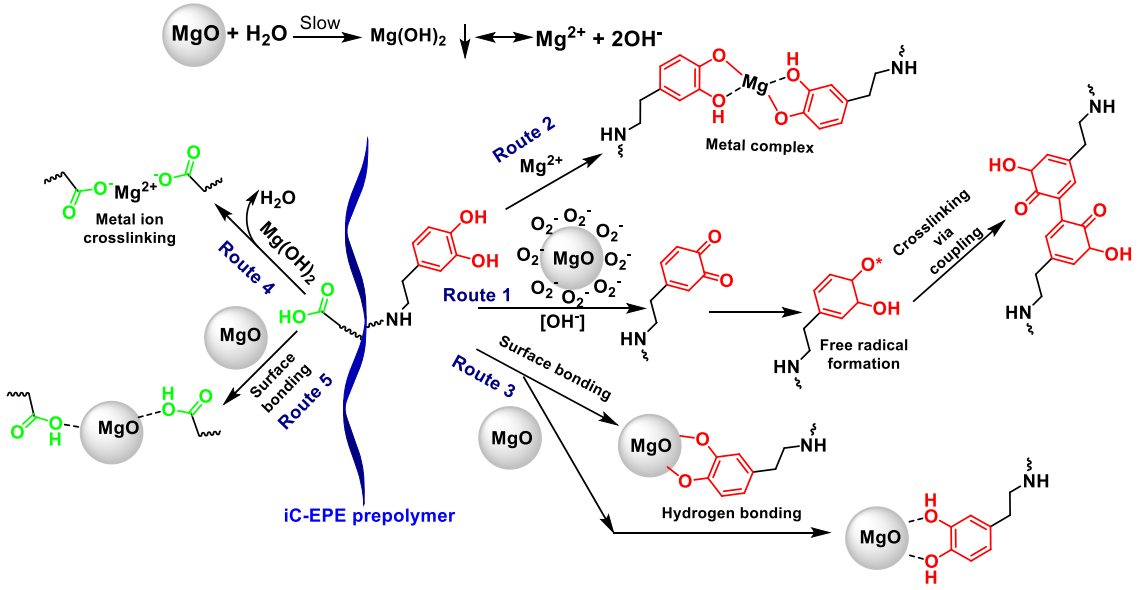

Scheme 2. Multifaceted crosslinking mechanisms of iC-EPE by MgO.

concentration increased to 4 wt%, the mutual inhibition effect between MgO and PI may be more prominent. When the PI concentration increased to 8 wt%, compared to that of 4 wt% PI, the gel time decreased again, except in the case of W15 + 8PI (W15 is defined as 15 wt% of MgO/composite with water as dispersion media for MgO particles; the nomenclature of different iC-EPE composite hydrogels are listed in Table 1), which might be attributed to relatively increased PI-induced crosslinking over MgO-induced crosslinking (Fig. 2C).

Rheology tests were conducted using representative samples, and the crossover points of the curves of storage modulus (G′) and loss modulus (G″) were determined to be the gel times (red circles in Fig. 2D, E and 2F) [17]. The gel times determined by rheology tests were comparable with that determined by tilting tests, proving that tilting tests is reliable and more convenient and easier to implement. From Fig. 2D, it can be seen that with the same amount of MgO used (10 wt% MgO), when the dispersion solvent of MgO was changed from ethanol to water, the gel time reduced from 558 s to 386 s, which is in agreement with the tilting test results (Fig. 2A). Fig. 2E further

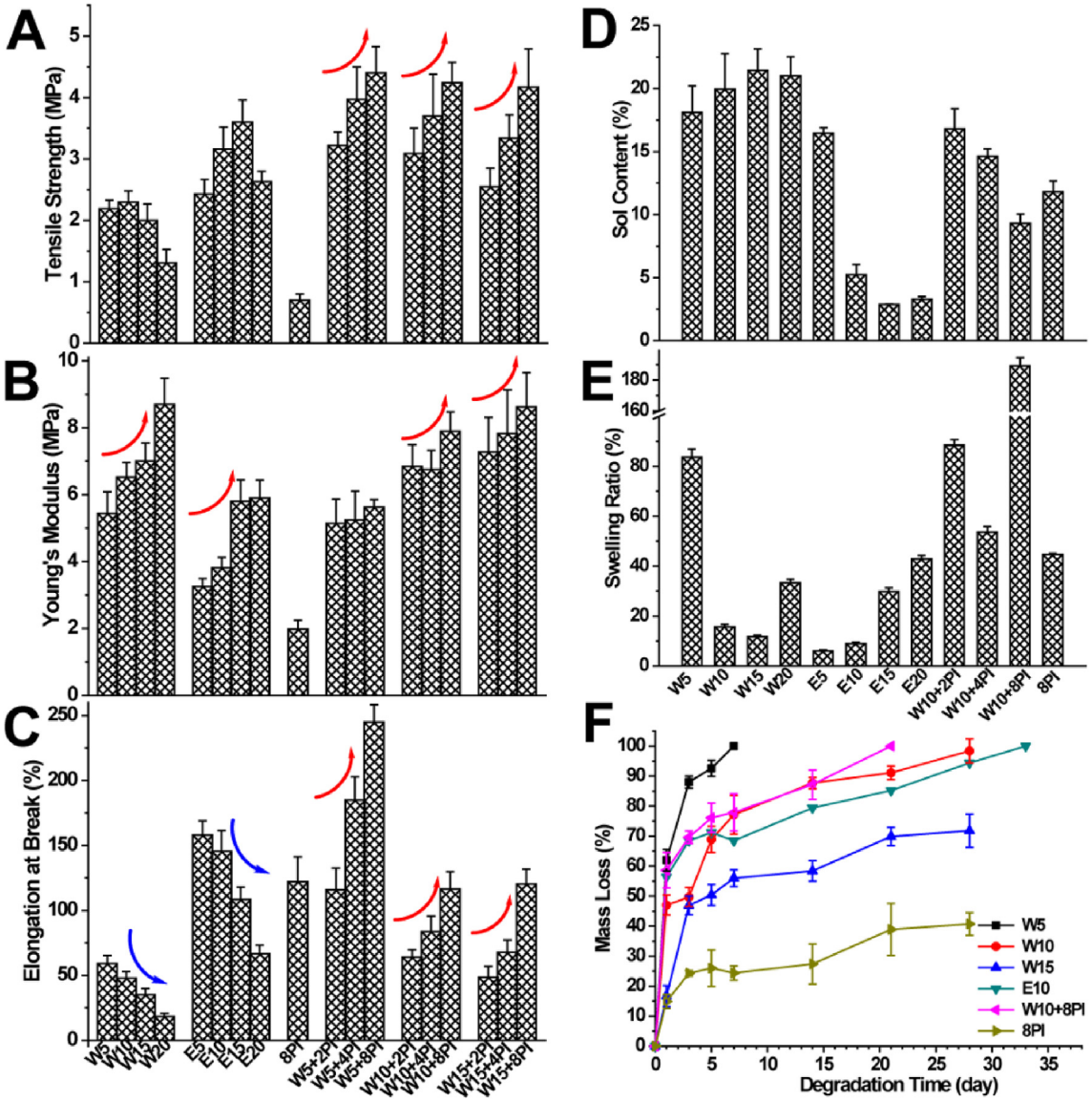

Fig. 3. Characterizations of crosslinked hydrogels: Mechanical, swelling, and degradation properties including tensile strength (**A**), initial modulus (**B**), elongation at break (**C**), sol content (**D**), swelling ratios (**E**), and degradation profiles (**F**) of iC-EPE bioadhesives crosslinked by MgO, MgO + PI or PI.

confirmed the same trend shown in Fig. 2B that the increase in temperature from RT (25 °C) to 37 °C led to the decrease in gel time. The synergistic effects between MgO and PI were also further confirmed by Fig. 2F that the gel time was vastly reduced from 386 s (W10, using 10 wt% MgO in water) to less than 10 s for W10 + 8PI (using 10 wt% MgO dispersed in 8 wt% PI solution).

3.3. Multifacted MgO crosslinking mechanism

The possible crosslinking mechanisms of MgO are exhibited in Scheme 2. The slow reaction between MgO and water to create a moderate alkaline condition seemed to be an essential step (Scheme 2). This could be deduced from the fact that without using any water in the formulation (with iC-EPE dissolved in ethanol and MgO dispersed in ethanol), iC-EPE/MgO could not crosslink, while using more water in the formula led to faster crosslinking (Table S1 and Fig. 2). The crosslinking mechanism of iC-EPE/MgO adhesives may be multifaceted: **1)** The reactive oxygen species (ROS), such as strong oxidative superoxide anions (O_2^-), on the surface of MgO particles induced the oxidation of catechol groups at alkaline conditions followed by free radical formation and crosslinking through coupling (route 1 in Scheme 2) [33,34]. The crystal defects of MgO particles may facilitate the formation of O_2^- on the surface of MgO [33,34]. The strong oxidizing capability of O_2^- on the surface of MgO particles at alkaline condition is also considered to be a reason for the antimicrobial activity of MgO [34]. Although overproduction of ROS at the inflamed area is believed to delay or interfere wound healing process, the inclusion of catechol-containing iC-EPE may serve as ROS scavenger to reduce the negative effects of ROS to wound healing [35]. And certain level of ROS was also previously proved to be beneficial to wound healing [36]. **2)** Metal complex formation between magnesium ions (Mg^{2+}) and catechol groups may also contribute to the crosslinking (route 2 in Scheme 2). **3)** Since iC-EPE prepolymer also contains free carboxyl (-COOH) groups, the reaction between $Mg(OH)_2$ (or possibly MgO) with –COOH groups and the formation of electrostatic interactions between Mg^{2+} and $-COO^-$ is also believed to contribute to crosslinking (route 4 in Scheme 2); however, ion bond formation between Mg^{2+} and $-COO^-$ should be very slow. This is supported by the inability to crosslink the –COOH–containing citrate-based prepolymer poly(poly(ethylene glycol) citrate) (PEGC, without catechol groups, synthesized by reacting CA and PEG according to our previous work [37]) with MgO (data not shown). **4)** Finally, the interactions between catechol groups or carboxyl groups with MgO

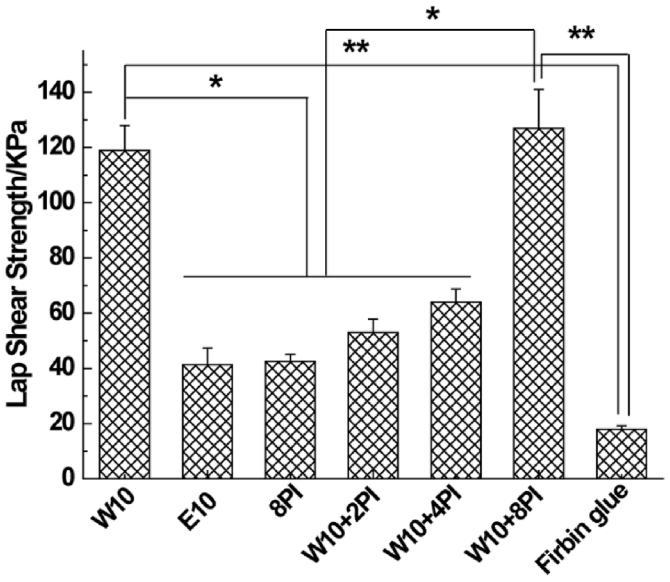

Fig. 4. Adhesion strength of iC-EPE crosslinked by MgO, PI or MgO + PI and fibrin glue to wet porcine small intestine submucosa measured by lap shear strength testing (*$p < 0.05$, **$p < 0.01$).

particles through surface bonding or hydrogen bonding (route 3 and 5 in Scheme 2) may serve as an additional way to crosslink.

In addition to triggering intermolecular crosslinking, oxidized catechol groups (ortho-quinone groups) also contribute to the strong adhesion to biological surfaces, through the formation of covalent bonds with nucleophile groups on tissue surfaces such as $–NH_2$, –SH, –OH and –COOH groups. The detailed mussel-inspired adhesion mechanisms have been discussed in our previous work [15].

3.4. Properties of cross-linked iC-EPE

To investigate the mechanical properties of the crosslinked iC-EPE composite hydrogels, tensile tests were carried out at both dry and wet conditions (Fig. 3 and Table S1). The tensile strengths of dried iC-EPE/MgO composite hydrogels, with/without PI, were in the range of 2–5 MPa, comparable with that of the previous iCMBAs crosslinked by PI which have tensile strengths ranging from 1 to 7.5 MPa [15]. Overall, in the tested formulations, increasing MgO content led to the increase of tensile strengths (Fig. 3A). The elastic moduli (Young's moduli) of crosslinked iC-EPE/MgO hydrogels increased gradually with the increase of the MgO content, whereas the elongation at break decreased (Fig. 3B and C). The tensile strengths and moduli of iC-EPE crosslinked by MgO or MgO + PI were much higher than that of the hydrogel crosslinked only by PI, demonstrating that MgO serves not only as a crosslinker, but also as a composite filler. The combination of MgO and PI not only enhanced the elastic moduli and tensile strengths but also increased the elongations at break. The stress-strain curves of crosslinked iC-EPE/MgO hydrogels are characteristic of elastomers, which is especially important for soft tissue applications in order to enable mechanical conformity and stress transfer between hydrogels and flexible and dynamic soft tissues (Fig. 3D). The mechanical properties of the crosslinked iC-EPE hydrogels in wet state are listed in Table S2. It can be seen that tensile strengths decreased when samples were hydrated

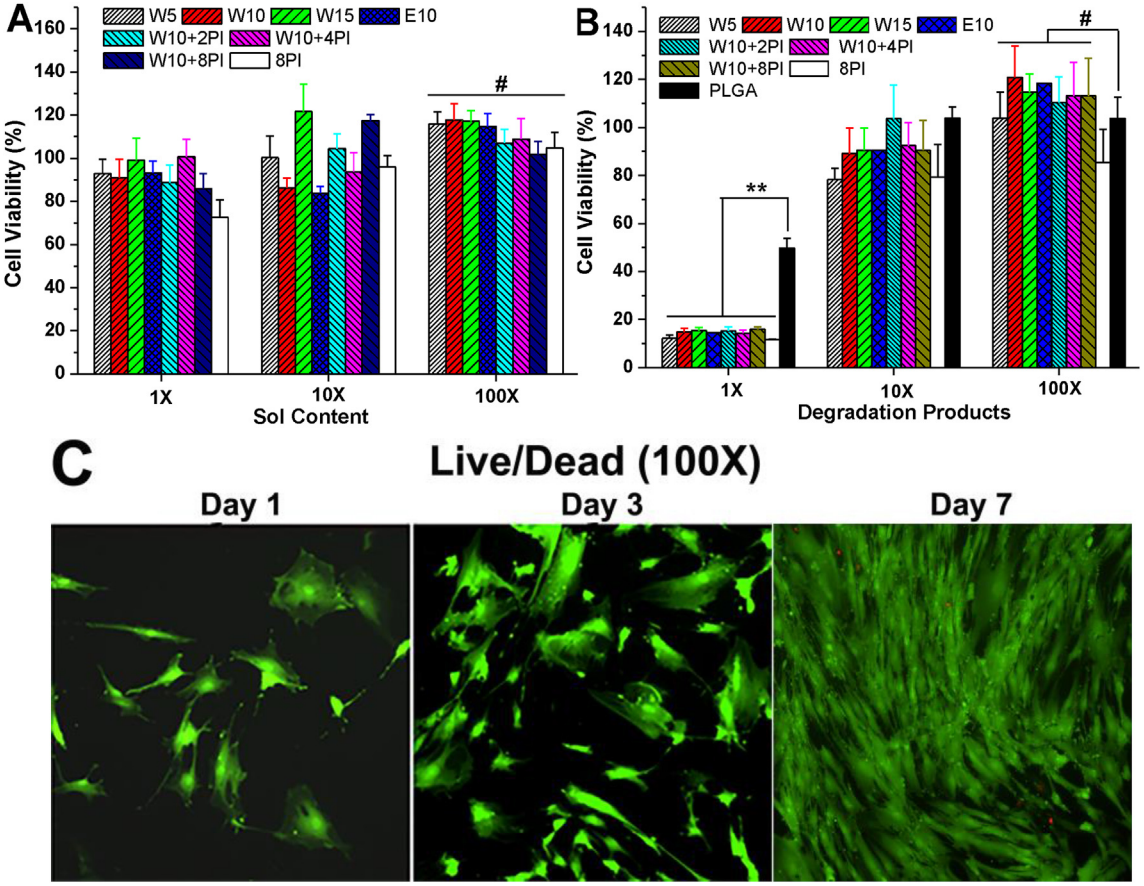

Fig. 5. Cytotoxicity evaluation of iC-EPE composite hydrogels: Cytotoxicity against human-derived mesenchymal stem cells (hMSC) by MTT assay for: leachants (sol content) (**A**) and degradation products (**B**) of iC-EPE composite hydrogels; Cell proliferation was assessed by Live/Dead assay of hMSCs seeded on MgO (10 wt%) crosslinked iC-EPE cast on glass slides 1, 3, and 7 days post cell seeding (**C**). $^{\#}p > 0.05$, **$p < 0.01$.

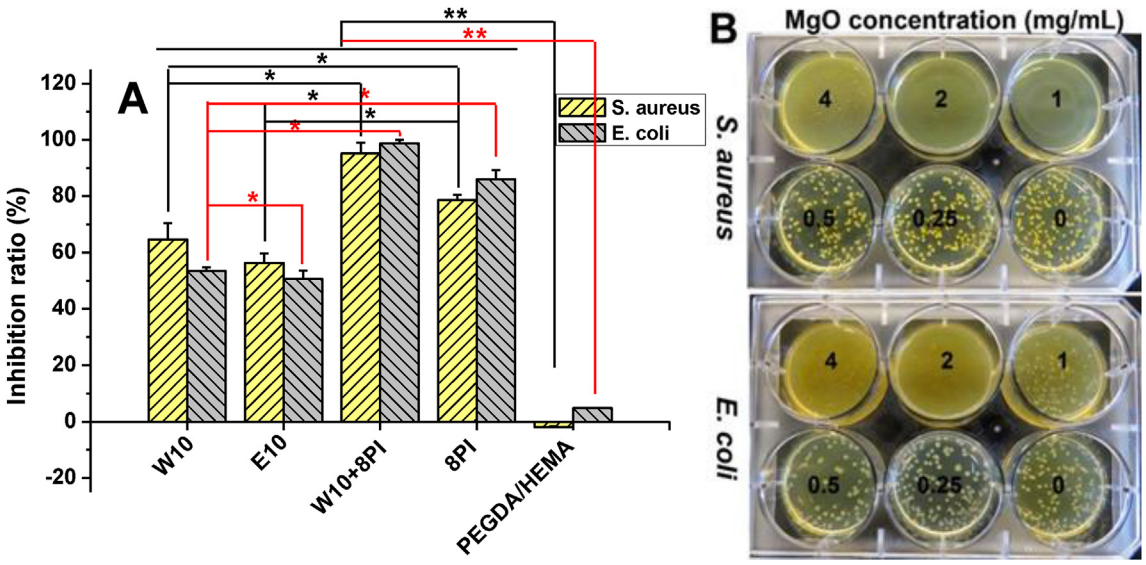

Fig. 6. Antibacterial efficacy: Bacterial inhibition ratios of iC-EPE-MgO hydrogels (0.5 g hydrogel in 5 mL bacteria containing broth) against *S. aureus* and *E. coli* (**A**); and *S. aureus* and *E. coli* growth images on agar gel with different MgO concentrations (the concentrations in mg/mL for MgO dispersed in agar gels in 6-well plates are labelled in black numbers) after 24 h incubation (**B**). $*p < 0.05$, $**p < 0.01$.

and swollen. These results suggest that the crosslinked iC-EPE hydrogels have tailorable mechanical properties for various clinical applications.

Sol contents of iC-EPE hydrogels crosslinked by MgO, MgO + PI or PI are shown in Fig. 3D. The sol contents of the tested formulae were all lower than 25%. The hydrogels crosslinked by MgO dispersion in ethanol possessed the lowest sol content, which was much lower than that of the hydrogel crosslinked by MgO dispersion in water or MgO + PI solution. This was attributed to the alkalinity of MgO, which might partially destroy the network of the hydrogels. As shown in Fig. 3E, the swelling ratios of iC-EPE hydrogels, crosslinked either by MgO (dispersed in water or ethanol), MgO + PI, or PI, were all lower than 200 wt %, with the lowest < 10 wt% (E5). The swelling ratios of EPE based iC formulae were all much lower than that of PEG-based iCMBAs (some > 1000 wt%), confirming the benefit of the replacement of hydrophilic PEG with more hydrophobic EPE.

Degradation of the crosslinked iC-EPE composite hydrogels was conducted at 37 °C in PBS and the mass losses at preset time points were recorded (Fig. 3F). iC-EPE hydrogels crosslinked by PI exhibited the slowest degradation rate with less than 40 wt% mass loss after 28 days. The hydrogels crosslinked by 5 wt% MgO dispersion in water exhibited the fastest degradation, with the degradation completed in 7 days. For the hydrogels crosslinked only by MgO, including W5, W10, W15, and E10, the degradation rate decreased with increased MgO content, implying that higher MgO content led to higher crosslinking density. Interestingly, iC-EPE crosslinked by 10 wt% MgO and 8 wt% PI (W10 + 8PI) degraded much faster than iC-EPE crosslinked only by 8 wt % PI (8PI) or by 10 wt% MgO (W10), supporting the mutual inhibition effect of MgO and PI on the crosslinking of iC-EPE prepolymer. The alkalinity of MgO in aqueous solution may also contribute to the accelerated degradation.

3.5. Adhesion strength

A preliminary assessment on the tissue adhesion strengths of iC-EPE/MgO bioadhesives was carried out by lap shear strength test under wet condition. The wet lap shear strengths of iC-EPE crosslinked by different crosslinking agents are shown in Fig. 4. The adhesion strengths of all tested formulae were higher than that of commercially available fibrin glue (15.4 ± 2.8 kPa) [15]. Although the iC-EPE hydrogels crosslinked by PI (8PI) or MgO/ethanol dispersion (E10) showed the lowest adhesion strengths, these values were still two fold that of fibrin glue. The iC-EPE hydrogel crosslinked by MgO and 8 wt% PI (W10 + 8PI) possessed the highest adhesion strength (127.0 ± 14.0 kPa). Lap shear strength not only reflects the adhesion strength to substrate, but is also closely related to the cohesion strength of the bioadhesive matrix. Thus, the lap shear strength test results further demonstrate that the incorporation of MgO improved the adhesion strengths and cohesion strengths of iC-EPE bioadhesives simultaneously. The adhesion strengths of iC-EPE/MgO system are superior to that of commercially available fibrin glue and are tunable by varying crosslinking agents.

3.6. In vitro cell viability and proliferation

The biocompatibility of iC-EPE hydrogels crosslinked by different crosslinking agents was estimated by conducting cytotoxicity studies of the soluble (leachable) contents and degradation products of various crosslinked iC-EPE hydrogels using MTT assay against human mesenchymal stem cells (hMSCs) (Fig. 5). The sol contents of iC-EPE hydrogels at 1 × concentration all demonstrated minor cytotoxicity, with hMSC viabilities higher than 80%, except 8PI. The cell viabilities of all tested samples increased in diluted solutions, with values close to or higher than 100% at 100 × diluted sol content (Fig. 5A). The 1 × degradation products showed much lower cell viabilities (< 20%) compared to PLGA (~50%). However, the cell viabilities of the 10 × and 100 × diluted solutions of degradation products became much higher, and were comparable to that of blank media and PLGA (Fig. 5B). The cytotoxicity of crosslinked iC-EPE hydrogels may arise from the release of MgO particles, residual PI, and its reduced components from the hydrogels. The proliferation of hMSCs on crosslinked iC-EPE films was also investigated using W10 as a representative sample by Live/Dead assay over three time points (1, 3 and 7 days) (Fig. 5C). It could be seen that hMSCs grew well and exhibited stretched/elongated morphology, indicating good cell attachment and proliferation on crosslinked iC-EPE films. These studies clearly indicate that the iC-EPE hydrogels crosslinked by MgO or MgO + PI were cytocompatible to hMSCs.

3.7. In vitro anti-bacterial performance

The antibacterial performance of the crosslinked iC-EPE hydrogels was assessed using *S. aureus* and *E. coli* as the most medically prevalent

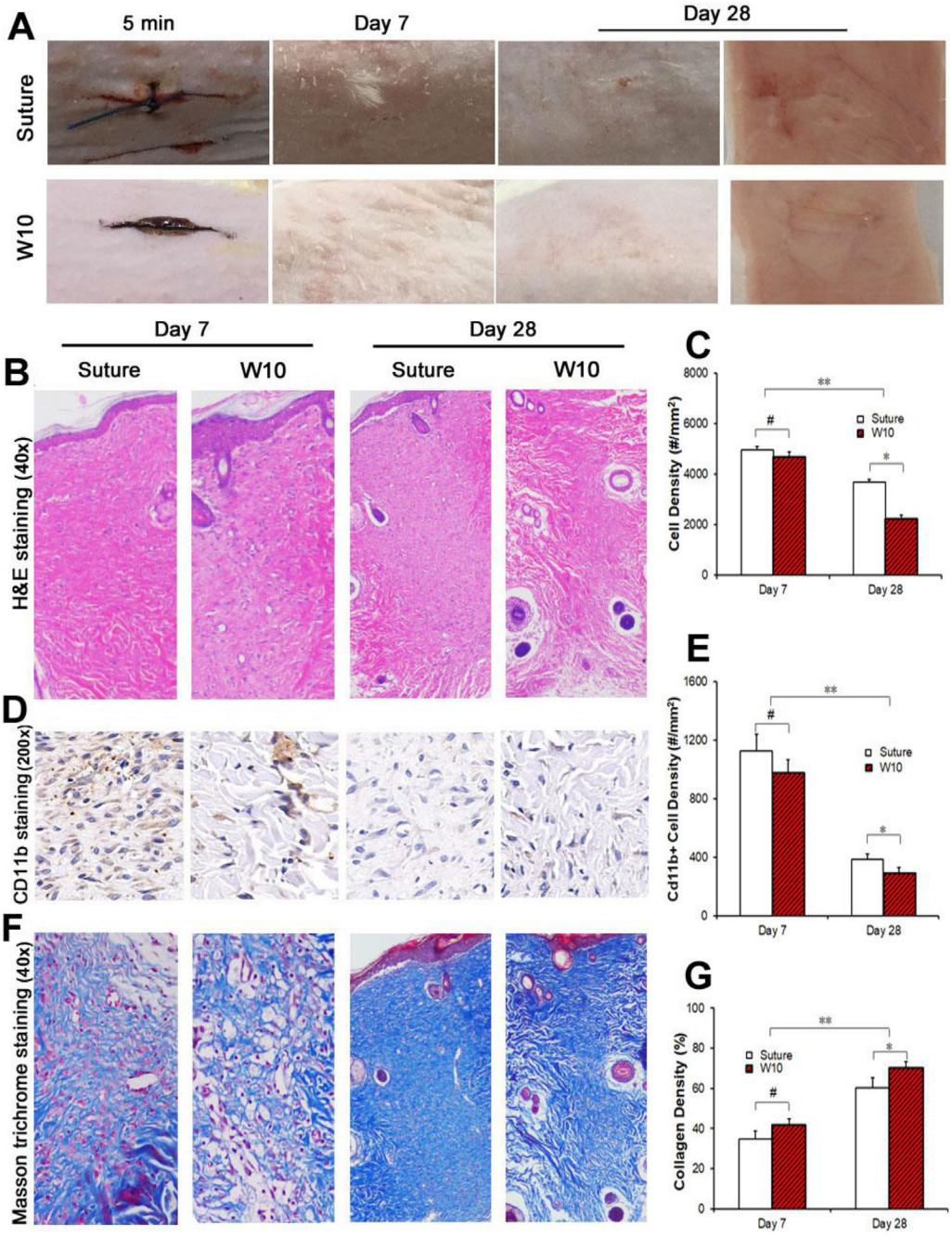

Fig. 7. *In vivo* evaluation on the biocompatibility and wound closure performance of iC-EPE-MgO (W10). (**A**) Gross observation of skin wounds treated with suture and W10 at different time points (5 min, 7 days and 28 days; the images of reverse side of the harvested skin samples near the treated wounds at day 28 are also shown on the right); H&E staining images (**B**) and the infiltrated cell densities in the incision areas (**C**) of the sutured group and the W10 groups; Images of CD11b immunohistochemical staining (**D**) and the numbers of CD11b positive cells around the wound areas of the sutured group and W10 group (**E**); Masson trichrome staining images (**F**) and the collagen densities in the wound areas of the sutured group and W10 group (**G**). $^{\#}p > 0.05$, $^{*}p < 0.05$, $^{**}p < 0.01$.

Gram-positive and Gram-negative bacteria, respectively, with PEGDA/HEMA as positive control [32]. The bacterial inhibition ratios of crosslinked iC-EPE against *S. aureus* and *E. coli* are shown in Fig. 6A. The iC-EPE hydrogels crosslinked by the combination of MgO and PI (W10 + 8PI, > 95%) exhibited the highest inhibition against both *S. aureus* and *E. coli* among the tested formulae. The hydrogels crosslinked only by PI (8PI, ~80%) displayed decreased inhibition, while the hydrogels crosslinked only by MgO (W10 and E10) exhibited the lowest bacteria inhibitions of around 60%. These results may be attributed to: **1)** PI released much faster than MgO particles because PI is a water-soluble small molecule, while MgO particles (micron sized) can only disperse in water; and **2)** PI itself possesses much stronger antibacterial effect than MgO particles, which could be seen from our previous work regarding the antibacterial performance of PI [16] and the antibacterial tests of MgO particles described in the following study (Fig. 6B).

In order to further certify the antibacterial property of MgO particles, the antibacterial performance of the MgO particles against *S. aureus* and *E. coli* was evaluated via an agar plate dilution method. Fig. 6B shows representative images for the bactericidal activities of the agar samples with different MgO concentrations. Clearly, higher MgO concentrations led to better antibacterial activity. Negligible bacteria colonies could be observed on the plates with MgO concentrations exceeding 1 mg/mL for *S. aureus* or 2 mg/mL for *E. coli*. These results suggest MgO had considerable antibacterial activity, and the bactericidal efficacy of MgO against *S. aureus* was greater than against *E. coli*.

A number of mechanisms have been proposed to explain the antibacterial performance of MgO particles, such as the formation of ROS like O_2^-, the interaction of MgO particles with bacteria followed by damage of bacterial cells, and an alkaline effect [34]. The antibacterial activity of iC-EPE/MgO bioadhesives may be beneficial in biomedical applications, where microbial infection is a significant challenge to overcome.

3.8. In vivo study

In order to further evaluate the biocompatibility and wound closure efficacy of iC-EPE crosslinked by MgO, *in vivo* study was conducted (Fig. 7). Upon applying iC-EPE/MgO (W10), the bleeding of incisions on Sprague-Dawley rats was immediately obstructed and an effective wound closure was achieved within 5 min (Fig. 7A). The application of W10 in the wounds generated a bulk adhesive chemically crosslinked/adhered to wound tissue via the mussel-inspired strategy [15], providing physical and mechanical barriers against blood loss. As proposed previously [15], abundant carboxyl groups on iC-EPE might also contribute a hemostatic effect. Furthermore, Mg^{2+} ions have been reported to play a role in the blood coagulation cascade [38–40]. The inclusion of Mg^{2+} releasing MgO particles could also lead to accelerated hemostat, another benefit of the iC-EPE/MgO adhesives. Ethanol in the solvent of iC-EPE serves as another hemostatic component [24–26], which also aided in bleeding control. Visual observation and comparison between the W10-treated wounds and the sutured wounds at different time points demonstrated high wound healing efficiency of iC-EPE. A diminished scar was observed for the W10-treated wounds compared to the sutured wounds at both day 7 and day 28 (Fig. 7A). Only minor acute inflammation was observed via histological evaluation (H & E staining) at day 7 when W10 was applied (Fig. 7B). Total cell density in the incision area of the W10-treated wounds (4691.7 ± 187.6 #/mm^2) showed no significant difference to that of the sutured wound (4975.0 ± 125.0 #/mm^2) at day 7 (Fig. 7C), while the total cell density of the wounds treated by W10 (2241.7 ± 142.2 #/mm^2) was noticeably less than that of the wounds treated by suturing (3691.7 ± 112.7 #/mm^2) at day 28 (Fig. 7C). Similarly, no significant difference between the W10-treated wounds (975.0 ± 90.1 #/mm^2) and the sutured wounds (1125.0 ± 114.6 #/mm^2) in the densities of CD11b positive cells in the incision areas at day 7 was detected (Fig. 7D and E), while, on day 28, the number of CD11b positive cells for the W10-treated wounds (291.7 ± 38.2 #/mm^2) was significantly less than that of the sutured wound (383.3 ± 38.1 #/mm^2, Fig. 7E), indicating the minimal inflammatory response of rats to W10. Furthermore, a higher amount of collagen expression was found at the sites of W10-treated wounds (day 7: 41.7%; day 28: 70.3%) than those treated with sutures (day 7: 34.7%; day 28: 60.3%), especially on day 28 (Fig. 7F and G). The above results suggest an excellent *in vivo* biocompatibility of iC-EPE crosslinked by MgO. The application of iC-EPE/MgO led to an improved and accelerated wound healing compared to suturing.

4. Conclusions

A family of hydrophobic citrate-based mussel-inspired tissue adhesives with greatly reduced swelling ratios were developed by simply reacting citric acid (CA), PEG-PPG-PEG diol, and dopamine (DP) in a one-pot reaction to form iC-EPE prepolymer, followed by crosslinking with biocompatible inorganic magnesium oxide (MgO) powder. Multifaceted crosslinking mechanisms involving MgO were discussed. Composite adhesives crosslinked by MgO (iC-EPE/MgO) exhibited high adhesion strengths, low swelling ratios, variable gel setting times, and tunable mechanical and degradation profiles. MgO serves not only as a crosslink initiator, but also as a composite filler, synergistically enhancing adhesion and cohesion. The iC-EPE/MgO bioadhesives demonstrated excellent *in vitro* and *in vivo* biocompatibility, notable antibacterial activity and superior hemostatic and wound closing efficacy. Given the biological beneficial of Mg ions in bone regeneration, iC-EPE/MgO composite adhesive hydrogels hold great promise as candidate materials for not only soft tissue wound closure but also hard tissue regeneration such as bone regeneration.

Declaration of competing interest

Dr. Yang and The Pennsylvania State University have a financial interest in Acuitive Technologies, Inc. and Aleo BME, Inc. These interests have been reviewed by the University's Institutional and Individual Conflict of Interest Committees and are currently being managed by the University.

Acknowledgements

None.

Appendix A. Supplementary data

Supplementary data to this article can be found online at https://doi.org/10.1016/j.biomaterials.2019.119719.

References

[1] D.A. Hickman, C.L. Pawlowski, U.D.S. Sekhon, J. Marks, A.S. Gupta, Biomaterials and advanced technologies for hemostatic management of bleeding, Adv. Mater. 30 (4) (2018) 1700859-1700899.
[2] D. Xie, J. Guo, M.R. Mehdizadeh, R.T. Tran, R. Chen, D. Sun, G. Qian, D. Jin, X. Bai, J. Yang, Development of injectable citrate-based bioadhesive bone implants, J. Mater. Chem. B. 3 (2015) 387–398.
[3] A.P. Duarte, J.F. Coelho, J.C. Bordado, M.T. Cidade, M.H. Gil, Surgical adhesives: systematic review of the main types and development forecast, Prog. Polym. Sci. 37 (8) (2012) 1031–1050.
[4] J. Li, A.D. Celiz, J. Yang, Q. Yang, I. Wamala, W. Whyte, B.R. Seo, N.V. Vasilyev, J.J. Vlassak, Z. Suo, D.J. Mooney, Tough adhesives for diverse wet surfaces, Science 357 (6349) (2017) 378–381.
[5] J. Guo, W. Sun, J.P. Kim, X. Lu, Q. Li, M. Lin, O. Mrowczynski, E.B. Rizk, J. Cheng, G. Qian, J. Yang, Development of tannin-inspired antimicrobial bioadhesives, Acta Biomater. 72 (2018) 35–44.
[6] N. Annabi, K. Yue, A. Tamayol, A. Khademhosseini, Elastic sealants for surgical applications, Eur. J. Pharm. Biopharm. 95 (2015) 27–39.
[7] T. Fattahi, M. Mohan, G.T. Caldwell, Clinical applications of fibrin sealants, J. Oral Maxillofac. Surg. 62 (2) (2004) 218–224.
[8] J.L. Lim, W.K. Lee, Enhanced biocompatibility and adhesive properties by aromatic amino acid-modified allyl 2-cyanoacrylate-based bio-glue, Colloids Surf., B 122 (2014) 669–673.
[9] J.R. Dusick, C.A. Mattozo, F. Esposito, D.F. Kelly, BioGlue for prevention of post-operative cerebrospinal fluid leaks in transsphenoidal surgery: a case series, Surg. Neurol. 66 (2006) 371–376.
[10] W. Furst, A. Banerjee, Conflict of interest disclosure relating to “Release of glutaraldehyde from an albumin-glutaraldehyde tissue adhesive causes significant in vitro and in vivo toxicity, Ann. Thorac. Surg. 79 (2005) 1522–1528.
[11] E.J. Beckman, M. Buckley, S. Agarwal, J. Zhang, US. 7264823B2, (2007).
[12] P.J.M. Bouten, M. Zonjee, J. Bender, S.T.K. Yauw, H. van Goor, J.C.M. van Hest, R. Hoogenboom, The chemistry of tissue adhesive materials, Prog. Polym. Sci. 39 (7) (2014) 1375–1405.
[13] G. Lee, C.K. Lee, M. Bynevelt, DuraSeal-hematoma: concealed hematoma causing spinal cord compression, Spine 35 (25) (2010) E1522–E1524.
[14] R. Wang, J. Li, W. Chen, T. Xu, S. Yun, Z. Xu, Z. Xu, T. Sato, B. Chi, H. Xu, A biomimetic mussel-inspired ε-poly-L-lysine hydrogel with robust tissue-anchor and anti-infection capacity, Adv. Funct. Mater. 27 (8) (2017) 1604894–1604907.
[15] M. Mehdizadeh, H. Weng, D. Gyawali, L. Tang, J. Yang, Injectable citrate-based mussel-inspired tissue bioadhesives with high wet strength for sutureless wound closure, Biomaterials 33 (32) (2012) 7972–7983.
[16] J. Guo, W. Wang, J. Hu, D. Xie, E. Gerhard, M. Nisic, D. Shan, G. Qian, S. Zheng, J. Yang, Synthesis and characterization of anti-bacterial and anti-fungal citrate-based mussel-inspired bioadhesives, Biomaterials 85 (2016) 204–217.
[17] J. Guo, G.B. Kim, D. Shan, J.P. Kim, J. Hu, W. Wang, F.G. Hamad, G. Qian, E.B. Rizk, J. Yang, Click chemistry improved wet adhesion strength of mussel-inspired citrate-based antimicrobial bioadhesives, Biomaterials 112 (2017) 275–286.
[18] Y. Liu, H. Meng, Z. Qian, N. Fan, W. Choi, F. Zhao, B.P. Lee, A moldable nanocomposite hydrogel composed of a mussel-inspired polymer and a nanosilicate as a fit-to-shape tissue sealant, Angew. Chem. Int. Ed. 56 (15) (2017) 4224–4228.
[19] Z. Gu, S. Li, F. Zhang, S. Wang, Understanding surface adhesion in nature: a peeling model, Adv. Sci. 3 (7) (2016) 1500327–1500340.
[20] D.G. Barrett, G.G. Bushnell, P.B. Messersmith, Mechanically robust, negative-swelling, mussel-inspired tissue adhesives, Adv. Healthc. Mater. 2 (5) (2013) 745–755.
[21] C. Ma, X. Tian, J.P. Kim, D. Xie, X. Ao, D. Shan, Q. Lin, M.R. Hudock, X. Bai, J. Yang, Citrate-based materials fuel human stem cells by metabonegenic regulation, Proc. Natl. Acad. Sci. U.S.A. 115 (50) (2018) E11741-E11750.
[22] D. Shan, S.-R. Kothapalli, D.J. Ravnic, E. Gerhard, J.P. Kim, J. Guo, C. Ma, J. Guo, L. Gui, L. Sun, D. Lu, J. Yang, Development of citrate-based dual-imaging enabled biodegradable electroactive polymers, Adv. Funct. Mater. 28 (34) (2018) 1801787.
[23] J. Guo, Z. Xie, R.T. Tran, D. Xie, D. Jin, X. Bai, J. Yang, Click chemistry plays a dual

role in biodegradable polymer design, Adv. Mater. 26 (12) (2014) 1906–1911.
[24] K. Sannier, A. Dompmartin, J. Théron, D. Labbé, M.T. Barrellier, R. Leroyer, P. Touré, D. Leroy, A new sclerosing agent in the treatment of venous malformations. Study on 23 cases, Interv. Neuroradiol. 10 (2) (2004) 113–127.
[25] M.M. Smith, M.P. Lin, R.V. Hovsepian, D. Wood, T. Nguyen, G.R.D. Evans, G.A. Wirth, Postoperative seroma formation after abdominoplasty with placement of continuous infusion local anesthetic pain pump, Can. J. Plast. Surg. 17 (4) (2009) 127–129.
[26] L. Cárdenas-Camarena, L.E. González, Large-volume liposuction and extensive abdominoplasty: a feasible alternative for improving body shape, Plast. Reconstr. Surg. 102 (5) (1998) 1698–1707.
[27] D.J. Hickey, B. Ercan, L. Sun, T.J. Webster, Adding MgO nanoparticles to hydroxyapatite-PLLA nanocomposites for improved bone tissue engineering applications, Acta Biomater. 14 (2015) 175–184.
[28] O. Yamamotoa, T. Ohira, K. Alvarez, M. Fukuda, Antibacterial characteristics of $CaCO_3$–MgO composites, Mater. Sci. Eng. B 173 (1–3) (2010) 208–212.
[29] Y. Rao, W. Wang, F. Tan, Y. Cai, J. Lu, X. Qiao, Influence of different ions doping on the antibacterial properties of MgO nanopowders, Appl. Surf. Sci. 284 (2013) 726–731.
[30] S. Sakai, K. Hirose, K. Taguchi, Y. Ogushi, K. Kawakami, An injectable, in situ enzymatically gellable, gelatin derivative for drug delivery and tissue engineering, Biomaterials 30 (20) (2009) 3371–3377.
[31] B.P. Lee, J.L. Dalsin, P.B. Messersmith, Synthesis and gelation of DOPA-modified poly(ethylene glycol) hydrogels, Biomacromolecules 3 (5) (2002) 1038–1047.
[32] L.C. Su, Z. Xie, Y. Zhang, K.T. Nguyen, J. Yang, Study on the antimicrobial properties of citrate-based biodegradable polymers, Front. Bioeng. Biotechnol. 2 (2014) 23.
[33] N.A. Vasil'eva, L.M. Plyasova, G.V. Odegova, Defective magnesium oxides with oxygen-containing anion fragments incorporated in the oxide structure, Kinet. Catal. 50 (6) (2009) 816–818.
[34] Z.-X. Tang, B.-F. Lv, MgO nanoparticles as antibacterial agent: preparation and activity, Braz. J. Eng Chem. 31 (3) (2014) 591–601.
[35] M. Mittal, M.R. Siddiqui, K. Tran, S.P. Reddy, A.B. Malik, Reactive oxygen species in inflammation and tissue injury, Antioxid.Redox Sign 20 (2014) 1126–1167.
[36] S. Xu, A.D. Chisholm1, C. Elegans epidermal wound induces a mitochondrial ROS burst that promotes wound repair, Dev. Cell 31 (2014) 48–60.
[37] D. Gyawali, P. Nair, Y. Zhang, R.T. Tran, C. Zhang, M. Samchukov, M. Makarov, H.K. Kim, J. Yang, Citric acid-derived in situ crosslinkable biodegradable polymers for cell delivery, Biomaterials 31 (34) (2010) 9092–9105.
[38] F. Sekiya, M. Yoshida, T. Yamashita, Magnesium(II) is a crucial constituent of the blood coagulation cascade. Potentiation of coagulant activities of factor IX by Mg^{2+} ions, J. Biol. Chem. 271 (15) (1996) 8541–8544.
[39] A.M.H.P. van den Besselaar, Magnesium and manganese ions accelerate tissue factor-induced coagulation independently of factor IX, Blood Coagul. Fibrinolysis 13 (1) (2002) 19–23.
[40] E.M. Liotta, S. Prabhakaran, R.S. Sangha, R.A. Bush, A.E. Long, S.A. Trevick, M.B. Potts, B.S. Jahromi, M. Kim, E.M. Manno, F.A. Sorond, A.M. Naidech, M.B. Maas, Magnesium, hemostasis, and outcomes in patients with intracerebral hemorrhage, Neurology 89 (8) (2017) 813–819.